Progress of Theoretical Physics, Vol. 126, No. 2, August 2011

On the Waterfall Behavior in Hybrid Inflation

Hideo KODAMA,[1,2] Kazunori KOHRI[1,2] and Kazunori NAKAYAMA[1]

[1] *Theory Center, Institute of Particle and Nuclear Studies, KEK, Tsukuba 305-0801, Japan*
[2] *Department of Particles and Nuclear Physics, The Graduate University for Advanced Studies, Tsukuba 305-0801, Japan*

(Received April 15, 2011; Revised June 3, 2011)

We revisit the hybrid inflation model focusing on the dynamics of the waterfall field in an analytical way. It is shown that inflation may last long enough during the waterfall regime for some parameter regions, confirming the claim of Clesse. In this case the scalar spectral index becomes red, and can fall into the best fit range of the WMAP observation.

Subject Index: 442

§1. Introduction

Inflation[1)] has become a standard scenario in the early Universe cosmology. It not only solves the horizon problem and flatness problem, but also explains the primordial density fluctuation of the Universe through the quantum fluctuation of the inflaton, which is a scalar field driving the inflationary expansion.

There are many models of inflation so far: new inflation,[2)] chaotic inflation,[3)] hybrid inflation,[4),5)] and so on. But it is still a challenging task to pin down the model observationally. This is partly because observational information is limited. What we extract from cosmological observations are the spectral index of the power spectrum of the density perturbation, n_S, and tensor-to-scalar ratio, r. Currently, the WMAP satellite combined with measurements of baryon acoustic oscillation and the present Hubble parameter constrains n_S as $n_S = 0.968 \pm 0.012$ with 68% C.L., and only an upper bound on r is given as $r < 0.24$ with 95% C.L.[6)] If future observations improve the accuracy of these parameters and find the evidence of primordial tensor perturbation, it will help us determine the correct inflation model. But even at the current level, some inflation models begin to be excluded. Generally, inflation models which predict blue spectral index, $n_S > 1$, are not favored from observational point of view.

The hybrid inflation is one of the models that predict blue spectral index, and hence people often consider that hybrid inflation models are on the verge of exclusion. In the hybrid inflation model, two scalar fields are introduced: one is the inflaton field ϕ and the other is the waterfall field ψ. The mass of the ψ is arranged so that it becomes tachyonic at some critical value of $\phi = \phi_c$, and inflation suddenly ends at this point. Recently, Ref. 7) argued that this picture might change for some cases, since inflation with large amount of e-foldings may still occur during the waterfall regime. In this case it is ψ, not ϕ, that actually takes a role of the inflaton relevant

for observational scales.

In this paper we revisit the hybrid inflation model, focusing on the detailed dynamics of the waterfall field. While Ref. 7) numerically investigated this topic, we analytically study the model in detail. We confirmed the claim of Ref. 7) and reproduced their results. For some parameter spaces, the waterfall field ψ causes the final 60 e-foldings of the inflationary expansion, which resembles new inflation or type I hilltop inflation scenario,[8),9)] and in this case the spectral index becomes red, on the contrary to the lore that the hybrid inflation predicts the blue spectral index.

The effects of the fluctuation of the waterfall field are also discussed recently.[10)–15)] In these studies, most of the 60 e-foldings are assumed to be spent before the waterfall regime. On the other hand, we are interested in the case that 60 e-foldings occurs during the waterfall regime. Thus our analysis is based on the classical dynamics of the ϕ and ψ, with some initial displacement ψ_0 at $\phi = \phi_c$. This is justified as long as one of the small patch with $\psi = \psi_0$ expands later and fills observable scales of the Universe due to subsequent inflationary expansion.

In the next section, we study the hybrid inflation model in detail in an analytical way, and calculate the scalar spectral index and tensor-to-scalar ratio.

§2. Dynamics of waterfall field

We introduce real scalar fields ϕ and ψ having the scalar potential of the following form:

$$V = \Lambda^4 \left[\left(1 - \frac{\psi^2}{v^2} \right)^2 + \frac{\phi^2}{\mu^2} + \frac{\phi^2 \psi^2}{w^4} \right]. \tag{2·1}$$

This kind of potential is often realized in supersymmetric (SUSY) theories.[16),17)] In SUSY case, ϕ and ψ should be regarded as complex scalars and $w = v$ holds.[*)] It is seen that the mass of the waterfall field ψ depends on the value of ϕ, and it becomes tachyonic at $\phi = \phi_c$, where

$$\phi_c = \frac{\sqrt{2} w^2}{v}. \tag{2·2}$$

Therefore, for $\phi > \phi_c$, ψ is stabilized at $\psi = 0$ and the potential for ϕ is flat and inflation occurs, and ψ begins to roll down the potential at $\phi = \phi_c$ towards the potential minimum $\phi = 0$ and $\psi = v$. In order for inflation to occur, $\mu \gg M_P$ is required, since otherwise ϕ rolls down too fast. Also we assume $v < M_P$ and $\phi_c < M_P$ in the following analysis. Otherwise, chaotic inflation takes place, as briefly discussed in the Appendix.

It is often assumed that this waterfall phase transition is sudden and inflation soon ends at $\phi = \phi_c$. In the following we will study the dynamics around the waterfall point in detail. Hereafter we define the "waterfall regime" as the region where $\phi < \phi_c$.

[*)] In SUSY, the potential is actually much more complicated due to the Coleman-Weinberg correction, supergravity correction, SUSY breaking effects. Correspondingly, the red spectral index is predicted for some parameter ranges.[17)–21)]

The equations of motion under the slow-roll approximation are given by

$$3H\dot{\phi} = -\frac{2\phi\Lambda^4}{\mu^2}\left(1+\frac{2\mu^2\psi^2}{v^2\phi_c^2}\right), \tag{2·3}$$

$$3H\dot{\psi} = -\frac{4\psi\Lambda^4}{v^2}\left(\frac{\phi^2-\phi_c^2}{\phi_c^2}+\frac{\psi^2}{v^2}\right). \tag{2·4}$$

Slow-roll parameters are directly calculated as

$$\epsilon_\phi = \frac{1}{2}M_P^2\left(\frac{V_\phi}{V}\right)^2 = \frac{2\phi^2M_P^2}{\mu^4}\left(1+\frac{2\mu^2\psi^2}{\phi_c^2v^2}\right)^2, \tag{2·5}$$

$$\epsilon_\psi = \frac{1}{2}M_P^2\left(\frac{V_\psi}{V}\right)^2 = \frac{8\psi^2M_P^2}{v^4}\left(\frac{\phi^2-\phi_c^2}{\phi_c^2}+\frac{\psi^2}{v^2}\right)^2, \tag{2·6}$$

$$\eta_{\phi\phi} = M_P^2\frac{V_{\phi\phi}}{V} = \frac{2M_P^2}{\mu^2}\left(1+\frac{2\mu^2\psi^2}{\phi_c^2v^2}\right), \tag{2·7}$$

$$\eta_{\phi\psi} = M_P^2\frac{V_{\phi\psi}}{V} = \frac{8\phi\psi M_P^2}{v^2\phi_c^2}, \tag{2·8}$$

$$\eta_{\psi\psi} = M_P^2\frac{V_{\psi\psi}}{V} = \frac{4M_P^2}{v^2}\left(\frac{\phi^2-\phi_c^2}{\phi_c^2}+\frac{3\psi^2}{v^2}\right). \tag{2·9}$$

Here $V_\phi \equiv \partial V/\partial\phi$ and so on, and $M_P = 2.4\times10^{18}$GeV is the reduced Planck scale. The true ends of inflation are at the point where the slow-roll conditions are violated, and what we are concerned is the dynamics between the critical point $\phi=\phi_c$ and this inflation end point.

2.1. *Classical solution*

For convenience, we parameterize ϕ and ψ as

$$\phi = \phi_c e^{\xi}, \quad \psi = \psi_0 e^{\chi}. \tag{2·10}$$

Thus, $\xi=\chi=0$ at the critical point and $\xi<0$ in the waterfall regime. We can set $|\xi|\ll1$ in all the following analyses. A typical initial displacement ψ_0 is of the order of the Hubble scale during inflation, $H_{\rm inf}\sim\Lambda^2/M_P$, because the ψ field is nearly massless around the critical point and obtains a quantum fluctuation. Hereafter, we follow the scalar dynamics classically with initial condition of $\psi=\psi_0$. In the case that sufficiently long inflation occurs during the waterfall regime, this treatment is justified because initially spatially small patch with $\psi=\psi_0$ covers the whole observable Universe. Actually results do not depend much on the value of ψ_0. Otherwise, effects of ψ on the curvature perturbation are more complicated. But still our analytical results are applied for small region of the Universe.

The scalar field dynamics at the waterfall regime is divided into three stages, which we call phase 0, phase 1 and phase 2 in the chronological order. The definitions of each stage are as follows.

- Phase 0 : The second term in Eq. (2·4) is dominant.
- Phase 1 : The first term in Eq. (2·4) is dominant.

• Phase 2 : The second term in Eq. (2·3) is dominant.

At the phase 0, the second term in Eq. (2·4) dominates the dynamics of ψ direction since $\phi \simeq \phi_c$ at the very beginning of the waterfall regime and the first term in Eq. (2·4) is neglected. Then ψ gradually decreases during this phase. For simplicity, we assume

$$\frac{\sqrt{2}\mu\psi_0}{\phi_c v} \ll 1, \tag{2·11}$$

as an initial condition, and the ϕ motion is determined by the first term in Eq. (2·3) at this stage. Thus ϕ also gradually decreases and begins to deviate from ϕ_c. At the phase 1, the first term in Eq. (2·4) becomes dominant and ψ increases, but still the second term in Eq. (2·3) is small enough to be neglected. Finally at the phase 2, the second term in Eq. (2·3) comes to dominate the dynamics of ϕ.

To be more precise, after the dynamics enters the phase 1, the second term in Eq. (2·4) again grows and scalar fields may reach the temporal minimum where the r.h.s. of Eq. (2·4) is zero. Then the scalar fields track the temporal minimum. This may happen at the phase 1 or phase 2 during the slow-roll regime, depending on parameters.

Slow-roll conditions are violated somewhere during these processes at $\phi = \phi_{\rm end}$, and it is not evident whether a large amount of e-folding number is spent for $\phi_{\rm end} < \phi < \phi_c$. In the following, we closely look into the dynamics of scalar fields at each of these stages and find the condition for which a sufficient amount of inflation takes place during the waterfall regime.

2.1.1. Phase 0

At this stage of the waterfall regime, slow-roll parameters are simplified as

$$\epsilon_\phi = \frac{2\phi^2 M_P^2}{\mu^4}, \tag{2·12}$$

$$\epsilon_\psi = \frac{8\psi^6 M_P^2}{v^8}, \tag{2·13}$$

$$\eta_{\phi\phi} = \frac{2M_P^2}{\mu^2}, \tag{2·14}$$

$$\eta_{\psi\psi} = \frac{12\psi^2 M_P^2}{v^4}. \tag{2·15}$$

Thus we assume $\psi_0 \ll v^{4/3} M_P^{-1/3}$ and $\psi_0 \ll v^2 M_P^{-1}$ so that slow-roll conditions are satisfied initially. The trajectory is determined from the slow-roll equation of motion, which can be rewritten as

$$\frac{d\xi}{d\chi} = \frac{v^4}{2\mu^2\psi_0^2} e^{-2\chi}. \tag{2·16}$$

Solving this equation, we obtain

$$\xi = \frac{v^4}{4\mu^2\psi_0^2}(1 - e^{-2\chi}). \tag{2·17}$$

From the slow-roll equation of motion

$$3H\dot{\xi} = -\frac{1}{\phi_c}\frac{\partial V}{\partial \phi}, \tag{2·18}$$

we find

$$\xi(N) = -\frac{2NM_P^2}{\mu^2}. \tag{2·19}$$

Here N counts the e-folding number after the critical point: $N = 0$ at the critical point and takes a positive value after that.

The phase 0 ends and enters the phase 1 at

$$\xi = -\frac{\psi_0^2}{2v^2}e^{2\chi}. \tag{2·20}$$

From Eqs. (2·17) and (2·20), we find that the phase 0 connects to phase 1 at

$$\xi_1 = \frac{v^4}{8\mu^2\psi_0^2}\left[1 - \sqrt{1 + \frac{8\mu^2\psi_0^4}{v^6}}\right], \tag{2·21}$$

$$\chi_1 = \frac{1}{2}\ln\left(-\frac{2v^2\xi_1}{\psi_0^2}\right). \tag{2·22}$$

Approximately we have

$$\xi_1 \simeq \begin{cases} -\dfrac{v}{2\sqrt{2}\mu} & \text{for} \quad \frac{8\mu^2\psi_0^4}{v^6} \gg 1 \\ -\dfrac{\psi_0^2}{2v^2} + \dfrac{\mu^2\psi_0^6}{v^8} & \text{for} \quad \frac{8\mu^2\psi_0^4}{v^6} \ll 1, \end{cases} \tag{2·23}$$

$$\chi_1 \simeq \begin{cases} -\dfrac{1}{2}\ln\left(\dfrac{v^3}{\sqrt{2}\mu\psi_0^2}\right) & \text{for} \quad \frac{8\mu^2\psi_0^4}{v^6} \gg 1 \\ -\dfrac{\mu^2\psi_0^4}{v^6} & \text{for} \quad \frac{8\mu^2\psi_0^4}{v^6} \ll 1. \end{cases} \tag{2·24}$$

Therefore, the e-folding number spent for the phase 0 is estimated as

$$N_0 = -\frac{\mu^2}{2M_P^2}\xi_1 \simeq \begin{cases} \dfrac{\mu v}{4\sqrt{2}M_P^2} & \text{for} \quad \frac{8\mu^2\psi_0^4}{v^6} \gg 1 \\ \dfrac{\mu^2\psi_0^2}{4M_P^2v^2} & \text{for} \quad \frac{8\mu^2\psi_0^4}{v^6} \ll 1. \end{cases} \tag{2·25}$$

Therefore the duration of phase 0 is sufficiently small for $\mu v \ll M_P^2$.

2.1.2. Phase 1

The phase 1 is defined as the region where the r.h.s. of Eq. (2·4) is dominated by the first term and

$$\frac{\sqrt{2}\mu\psi}{\phi_c v} \ll 1. \tag{2·26}$$

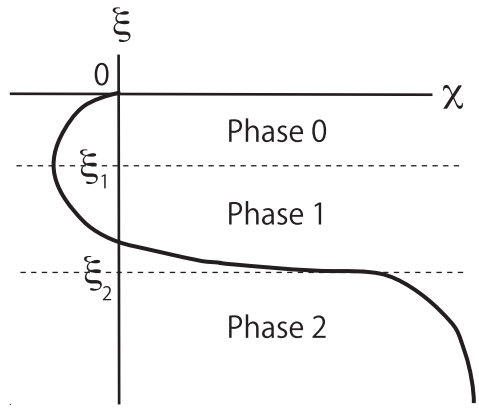

Fig. 1. Schematic picture for the trajectory of the ξ and χ.

At this stage of the waterfall regime, slow-roll parameters are simplified as

$$\epsilon_\phi = \frac{2\phi^2 M_P^2}{\mu^4}, \tag{2·27}$$

$$\epsilon_\psi = \frac{8\psi^2 M_P^2}{v^4}\left(\frac{\phi^2-\phi_c^2}{\phi_c^2}\right)^2 \sim \frac{32\psi^2 M_P^2 \xi^2}{v^4}, \tag{2·28}$$

$$\eta_{\phi\phi} = \frac{2M_P^2}{\mu^2}, \tag{2·29}$$

$$\eta_{\psi\psi} = \frac{4M_P^2}{v^2}\left(\frac{\phi^2-\phi_c^2}{\phi_c^2}\right) \sim \frac{8M_P^2\xi}{v^2}. \tag{2·30}$$

We find the trajectory of the scalar fields from the relation

$$\frac{d\xi}{d\chi} = \frac{v^2}{4\mu^2\xi}, \tag{2·31}$$

which is derived from the equation of motion. Matching to the phase 0 solution at $\xi = \xi_1$, we find that χ is given by

$$\xi^2 = \xi_1^2 + \frac{v^2}{2\mu^2}(\chi - \chi_1). \tag{2·32}$$

The phase 1 connects to phase 2 at $\chi = \chi_2$ defined by

$$\frac{\sqrt{2}\mu\psi_0 e^{\chi_2}}{\phi_c v} = 1 \leftrightarrow \chi_2 = \ln\left(\frac{\phi_c v}{\sqrt{2}\mu\psi_0}\right). \tag{2·33}$$

From the assumption (2·11), we have $\chi_2 > 0$.

Here we must check whether the assumption that the second term in Eq. (2·4) is negligible during the phase 1 ($|\xi_1| < |\xi| < |\xi_2|$). If the second term in Eq. (2·4) again becomes efficient, the ψ field is trapped at the temporal minimum of the potential, and then tracks the temporal minimum after that. The trajectory of the temporal

minimum, $\partial V/\partial\psi = 0$, is given by

$$\xi = -\frac{\psi_0^2}{2v^2}e^{2\chi}. \tag{2·34}$$

Let us denote the point where the trajectory (2·32) crosses the temporal minimum (2·34) by ξ_{*1}. If $|\xi_{*1}| > |\xi_2|$, the fields do not reach the temporal minimum before they enter in the phase 2. This condition is rewritten as

$$\chi_2 > \frac{\phi_c^4}{8\mu^2 v^2}. \tag{2·35}$$

If this is satisfied, the trajectory (2·32) is valid during the phase 1. In this case we have $\xi_2 = -cv/\mu$ with $c = \sqrt{\chi_2/2}$: we call this case phase 1-(a). Otherwise, the fields are trapped at the temporal minimum of the potential at $\xi = \xi_{*1}$ which satisfies $|\xi_1| < |\xi_{*1}| < |\xi_2|$: we call this case phase 1-(b). In this case the trajectory is given by Eq. (2·34) for $|\xi| > |\xi_{*1}|$, and we have $\xi_2 = -\phi_c^2/(4\mu^2)$.

To summarize, the phase 1-(a) trajectory is given by

$$\xi^2 = \xi_1^2 + \frac{v^2}{2\mu^2}(\chi - \chi_1) \quad \text{for} \quad |\xi_1| < |\xi| < |\xi_2|, \tag{2·36}$$

where $\xi_2 = -cv/\mu$ if $\chi_2 > \phi_c^4/(8\mu^2 v^2)$, and the phase 1-(b) trajectory is given by

$$\xi^2 = \xi_1^2 + \frac{v^2}{2\mu^2}(\chi - \chi_1) \quad \text{for} \quad |\xi_1| < |\xi| < |\xi_{*1}|, \tag{2·37}$$

$$\xi = -\frac{\psi_0^2}{2v^2}e^{2\chi} \quad \text{for} \quad |\xi_{*1}| < |\xi| < |\xi_2|, \tag{2·38}$$

where $\xi_2 = -\phi_c^2/(4\mu^2)$ if $\chi_2 < \phi_c^4/(8\mu^2 v^2)$.

The e-folding number during the phase 1 is also estimated from the same equation of motion (2·18). In the phase 1, we obtain

$$\xi(N) = \xi_1 - \frac{2M_P^2}{\mu^2}(N - N_0). \tag{2·39}$$

Therefore the e-folding number during the phase 1 is given by

$$\Delta N_1 = N_1 - N_0 = \frac{\mu^2}{2M_P^2}(\xi_1 - \xi_2). \tag{2·40}$$

Here N_1 is given by

$$N_1 \simeq \begin{cases} \dfrac{\sqrt{\chi_2}}{2\sqrt{2}}\dfrac{\mu v}{M_P^2} & \text{for} \quad \chi_2 > \frac{\phi_c^4}{8\mu^2 v^2}, \\ \dfrac{1}{8}\dfrac{\phi_c^2}{M_P^2} & \text{for} \quad \chi_2 < \frac{\phi_c^4}{8\mu^2 v^2}. \end{cases} \tag{2·41}$$

Thus we need at least $\mu v \gg M_P^2$ for long enough inflation to occur at this stage.

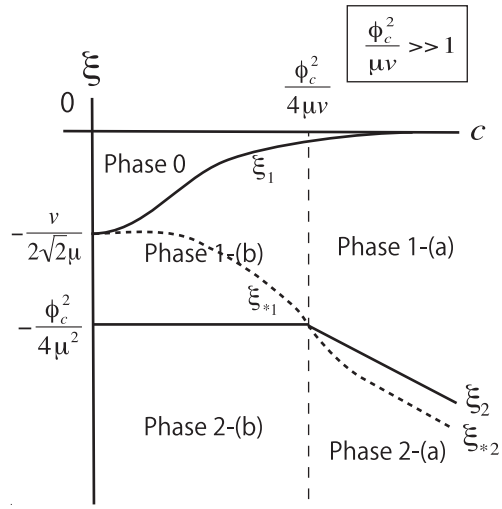

Fig. 2. Schematic presentation of the classification of phase 0-2 for $\phi_c^2/(\mu v) \gg 1$. The horizontal axis is $c = \sqrt{\chi_2/2}$ where χ_2 is defined by Eq. (2·33). The vertical axis is ξ, which starts from 0 and moves down on the figure perpendicularly. The dotted line represents ξ_{*1} and ξ_{*2}, below which scalars are trapped by the temporal minimum.

One can easily find that at $N \sim \mu v/M_P^2$, χ becomes close to unity if $\chi_2 \sim \mathcal{O}(1) > \phi_c^4/(8\mu^2 v^2)$. Then, ψ exponentially grows up, and the approximation (2·26) soon breaks down, hence it goes into the second stage. At this transition point $N \sim \mu v/M_P^2$, $\eta_{\psi\psi} \sim -8M_P^2/(\mu v)$. Thus inflation does not end at the first stage of the waterfall regime as long as $\mu v \gg 8M_P^2$. In the opposite case $\mu v \ll 8M_P^2$, inflation terminates at $\xi = -M^2/8M_P^2$ during this stage. But in this case, the e-folding number during the waterfall regime is estimated as $N = \mu^2 v^2/(16M_P^4) \lesssim 1$. Thus, in order for sufficient inflation to occur during the waterfall regime, we need at least $\mu v \gg 8M_P^2$. In the opposite case $\chi_2 < \phi_c^4/(8\mu^2 v^2)$, the duration is sufficiently short as long as $\phi_c \ll M_P$.

2.1.3. Phase 2

The phase 2 is defined as the region where

$$\frac{\sqrt{2}\mu\psi}{\phi_c v} \gg 1. \tag{2·42}$$

At this stage, slow-roll parameters are given by

$$\epsilon_\phi \simeq \frac{8M_p^2\psi^4}{\phi_c^2 v^4}, \tag{2·43}$$

$$\epsilon_\psi \simeq \frac{32\psi^2 M_P^2 \xi^2}{v^4}, \tag{2·44}$$

$$\eta_{\phi\phi} \simeq \frac{4M_P^2\psi^2}{\phi_c^2 v^2}, \tag{2·45}$$

$$\eta_{\psi\psi} \simeq \frac{8M_P^2\xi}{v^2}. \tag{2·46}$$

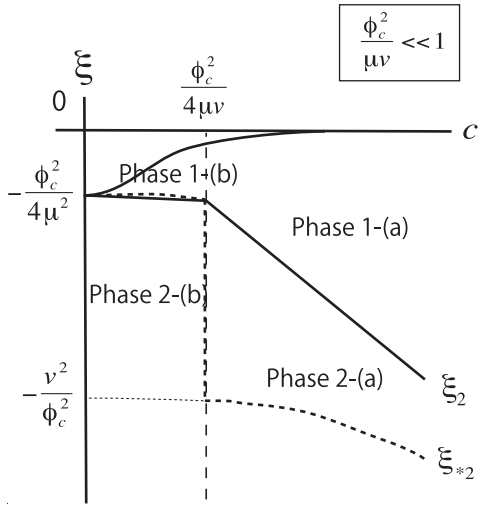

Fig. 3. Same as Fig. 2, but for $\phi_c^2/(\mu v) \ll 1$.

We can also solve the slow-roll equation of motion at this stage. In this limit, the scalar field trajectory is found from the relation

$$\frac{d\xi}{d\chi} = \frac{\psi_0^2}{2\phi_c^2}\frac{e^{2\chi}}{\xi}. \tag{2·47}$$

Matching to the phase 1 at $(\xi, \chi) = (\xi_2, \chi_2)$, we obtain

$$\xi^2 = \xi_2^2 + \frac{v^2}{4\mu^2}\left[e^{2(\chi-\chi_2)} - 1\right]. \tag{2·48}$$

As already described, if $\chi_2 < \phi_c^4/(8\mu^2 v^2)$, the fields are trapped at the temporal minimum before entering the phase 2, and the trajectory (2·20) connects to the phase 2 : we call this case phase 2-(b). For $\chi_2 > \phi_c^4/(8\mu^2 v^2)$, the phase 1-(a) trajectory (2·32) connects to the phase 2 : we call this case phase 2-(a). Even for the phase 2-(a), there is a possibility that the fields are trapped by the temporal minimum before inflation ends. From the trajectory (2·48) and the temporal minimum (2·20), we find that the phase 2 trajectory crosses the temporal minimum at $\xi = \xi_{*2}$, where

$$\xi_{*2} = -\frac{v^2}{2\phi_c^2}\left[1 + \sqrt{1 + (2\chi_2 - 1)\frac{\phi_c^4}{\mu^2 v^2}}\right]. \tag{2·49}$$

Therefore, approximately we have

$$\xi_{*2} \simeq \begin{cases} -\dfrac{v^2}{\phi_c^2} & \text{for } \frac{\phi_c^4}{\mu^2 v^2} < \chi_2 < \frac{\mu^2 v^2}{\phi_c^4}, \\ -\sqrt{\dfrac{\chi_2}{2}}\dfrac{v}{\mu} - \dfrac{v^2}{2\phi_c^2}\ (\lesssim \xi_2) & \text{otherwise.} \end{cases} \tag{2·50}$$

To summarize, the phase 2-(a) trajectory is given by

$$\xi^2 = \xi_2^2 + \frac{v^2}{4\mu^2}\left[e^{2(\chi-\chi_2)} - 1\right] \text{ for } |\xi_2| < |\xi| < |\xi_{2*}|, \tag{2·51}$$

$$\xi = -\frac{\psi_0^2}{2v^2}e^{2\chi} \quad \text{for} \quad |\xi_{2*}| < |\xi|, \tag{2·52}$$

where $\xi_2 = -cv/\mu$ if $\chi_2 > \phi_c^4/(8\mu^2 v^2)$, and the phase 2-(b) trajectory is given by

$$\xi = -\frac{\psi_0^2}{2v^2}e^{2\chi} \quad \text{for} \quad |\xi_2| < |\xi|, \tag{2·53}$$

where $\xi_2 = -\phi_c^2/(4\mu^2)$ if $\chi_2 < \phi_c^4/(8\mu^2 v^2)$, until the slow-roll conditions are violated. Figures 2 and 3 schematically represent these classifications. The horizontal axis is $c = \sqrt{\chi_2/2}$ and the vertical axis is ξ, which starts from 0 and moves down on the figure perpendicularly. The dotted line represents ξ_*, under which scalars are trapped by the temporal minimum. For example, in Fig. 2, we can see that the fields are trapped by the temporal minimum when it traverses the dotted line before reaching the phase 2 regime for $c \ll \phi_c^2/(\mu v)$. This corresponds to the phase 1-(b).

Using the trajectory (2·48), the slow-roll equation of motion becomes

$$3H\dot{\xi} = -\frac{8\Lambda^4}{v^2}\left(\xi^2 - \xi_2^2 + \frac{v^2}{4\mu^2}\right). \tag{2·54}$$

If $\chi_2 > 1/2$, it can be solved analytically as

$$\xi(N) = \frac{-(c'-c)f(N) + c' + c}{(c'-c)f(N) + c' + c}\xi_2', \tag{2·55}$$

where $c = \sqrt{\chi_2/2}$, $\xi_2' = -c'v/\mu$ with $c' = \sqrt{c^2 - 1/4}$ and

$$f(N) = \exp\left(\frac{16c'M_P^2}{\mu v}(N - N_1)\right). \tag{2·56}$$

Note that this expression for $\xi(N)$ diverges ($\xi \to -\infty$) at $N = N_{\rm div}$, where

$$N_{\rm div} = N_1 + \frac{\mu v}{16M_P^2 c'}\ln\left(\frac{c+c'}{c-c'}\right). \tag{2·57}$$

Before reaching this point, the slow-roll conditions are violated at $N = N_{\rm end}$, where $N_{\rm end}$ is defined at the point where $\eta_{\psi\psi} = -1$ and $\xi = \xi_{\rm end}$ with

$$\xi_{\rm end} = -\frac{v^2}{8M_P^2}. \tag{2·58}$$

Explicitly, it is expressed as

$$N_{\rm end} = N_1 + \frac{\mu v}{16M_P^2 c'}\ln\left(\frac{\xi_{\rm end} - \xi_2'}{\xi_{\rm end} + \xi_2'}\frac{c+c'}{c-c'}\right). \tag{2·59}$$

If the trajectory reaches temporal minimum before inflation ends, the inflation end point is given by

$$\xi_{\rm end} = \begin{cases} -\dfrac{\phi_c^2}{8M_P^2} & \text{for } v > \sqrt{2}\phi_c, \\ -\dfrac{v^2}{16M_P^2} & \text{for } v < \sqrt{2}\phi_c. \end{cases} \tag{2·60}$$

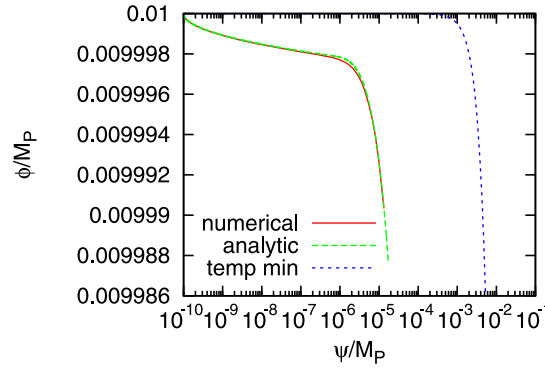

Fig. 4. Trajectory of the ϕ and ψ fields. We have taken $v = 0.1M_P, \phi_c = 0.01M_P, \mu = 10^3 M_P$ and $\psi_0 = 10^{-10} M_P$. This case corresponds to the Phase 1-(a) - Phase 2-(a) solution in Fig. 3. Our analytic solution fits very well with the numerical result. For comparison, the track of the temporal minimum is also shown.

To summarize, the ξ evolves as a function of N as

$$\xi(N) = -\frac{2M_P^2 N}{\mu^2} \quad \text{for} \quad |\xi| < |\xi_2|,$$
$$\xi(N) = \frac{-(c'-c)f(N) + c' + c}{(c'-c)f(N) + c' + c}\xi_2' \quad \text{for} \quad |\xi_2| < |\xi| < |\xi_{\rm end}|. \tag{2·61}$$

A trajectory is shown in Fig. 4. We have taken $v = 0.1M_P, \phi_c = 0.01M_P, \mu = 10^3 M_P$ and $\psi_0 = 10^{-10} M_P$. This case corresponds to the Phase 1-(a) - Phase 2-(a) solution in Fig. 3. It is seen that our analytic solution fits very well with the numerical result. Figures 5 and 6 show trajectories of the ϕ and ψ, respectively, as a function of N.

A trajectory for another set of parameters is shown in Fig. 7. We have taken $v = 10^{-5} M_P, \phi_c = 0.1M_P, \mu = 100M_P$ and $\psi_0 = 10^{-10} M_P$. This case corresponds to the Phase 1-(b) - Phase 2-(b) solution in Fig. 2. It is seen that the trajectory tracks the temporal minimum.

From Eq. (2·59), we can see that in order to have enough amount of inflation after waterfall, the following condition must be satisfied:

$$N_{\rm end} \sim N_1 > N_e(\sim 60) \leftrightarrow \mu M > 2N_e M_P^2. \tag{2·62}$$

This agrees with the result of Clesse.[7] Thus in this limit, the last N_e e-folds is obtained during the waterfall regime and actually the waterfall field ψ should be regarded as the inflaton. It resembles new inflation or type I hilltop model.[8] In the opposite limit, the waterfall phase transition occurs suddenly and the model approaches the standard hybrid inflation model.

2.2. *Spectral index*

Now, we evaluate the spectral index in this model. First, we must identify the position of the inflaton, $\xi = \xi(N_{\rm end} - N_e)$, when observable scales left the horizon.

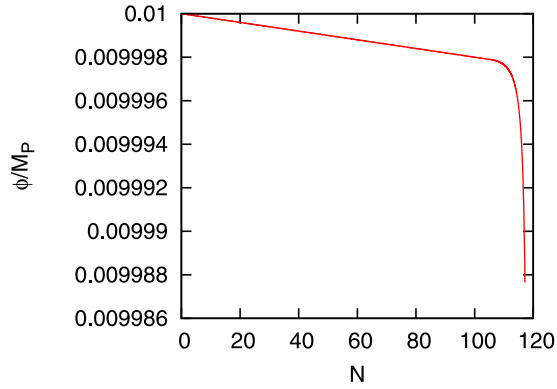

Fig. 5. The ϕ as a function of N. Parameters are the same as those in Fig. 4.

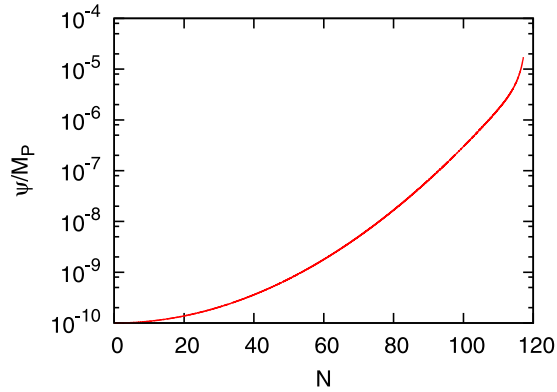

Fig. 6. The ψ as a function of N. Parameters are the same as those in Fig. 4.

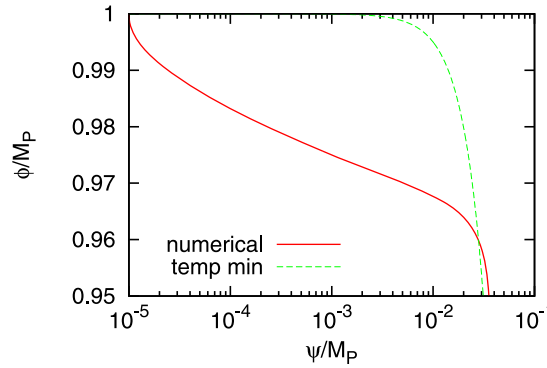

Fig. 7. Trajectory of the ϕ and ψ fields. We have taken $v = 10^{-5}M_P$, $\phi_c = 0.1M_P$, $\mu = 100M_P$ and $\psi_0 = 10^{-10}M_P$. This case corresponds to the Phase 1-(b) - Phase 2-(b) solution in Fig. 2. It is seen that the solution tracks the temporal minimum.

It is given by

$$\xi(N_{\rm end}-N_e)=\frac{-(c'-c)f(N_{\rm end}-N_e)+c'+c}{(c'-c)f(N_{\rm end}-N_e)+c'+c}\xi_2', \tag{2·63}$$

if inflation lasts long enough at $|\xi|>|\xi_2|$, or $N_{\rm end}>N_1+N_e$. Otherwise, if $N_{\rm end}<N_1+N_e$, we obtain

$$\xi(N_{\rm end}-N_e)=-\frac{2M_P^2(N_{\rm end}-N_e)}{\mu^2}. \tag{2·64}$$

In this model, both ϕ and ψ slowly roll down the scalar potential and hence the adiabatic field σ, which is responsible for the curvature perturbation, should be a combination of these fields. The scalar spectral index in this case is calculated from[22),23)]

$$n_S=1-6\epsilon_\sigma(N_e)+2\eta_{\sigma\sigma}(N_e), \tag{2·65}$$

where we have defined slow-roll parameters for the adiabatic field σ as

$$\epsilon_\sigma=\epsilon_\phi+\epsilon_\psi, \tag{2·66}$$

and

$$\eta_{\sigma\sigma}=\eta_{\phi\phi}\cos^2\theta+2\eta_{\phi\psi}\sin\theta\cos\theta+\eta_{\psi\psi}\sin^2\theta. \tag{2·67}$$

Here, the adiabatic field σ is given by

$$\dot\sigma=\dot\phi\cos\theta+\dot\psi\sin\theta, \tag{2·68}$$

where

$$\cos\theta=\frac{\dot\phi}{\sqrt{\dot\phi^2+\dot\psi^2}},\quad \sin\theta=\frac{\dot\psi}{\sqrt{\dot\phi^2+\dot\psi^2}}. \tag{2·69}$$

Since we already know the analytic solution of the inflaton trajectory, it is a straightforward task to calculate the scalar spectral index.

Contours of n_S are shown in Fig. 8. It is seen that in the limit (2·62), the spectral index becomes red, because the final 60 e-foldings is in the hilltop inflation regime, where the ψ field has a negative curvature. In the opposite limit, it becomes slightly blue since the ϕ field causes inflation before the critical point and it has a positive curvature.

A scalar degree of freedom perpendicular to σ also has quantum fluctuations and it is an isocurvature mode.[24)] Whether such an isocurvature mode contributes to the final density perturbation or not depends on the physics of reheating after inflation. We do not go into detail of this aspect since it is strongly model dependent. In the simplest case where both ϕ and ψ decay into radiation quickly after inflation, the isocurvature mode has no physical importance.

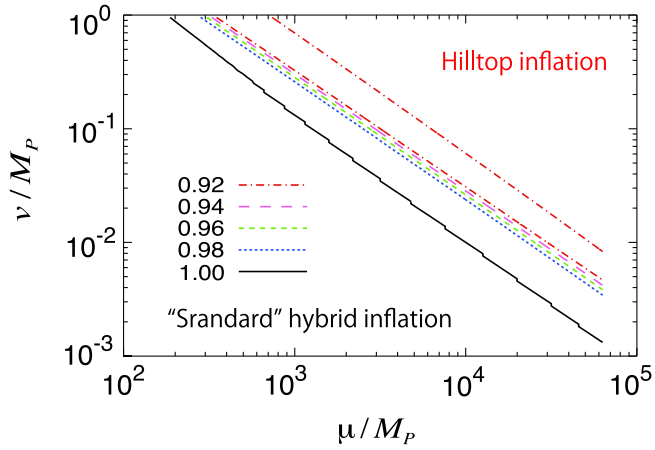

Fig. 8. Contours of the scalar spectral index n_S on (μ, v)-plane. We have taken $\phi_c = 10^{-3}M_P$ and $\psi_0 = 10^{-15}M_P$. The whole region corresponds to the case of Phase 1-(a) - Phase 2-(a) solution in Fig. 3.

2.2.1. Hilltop inflation limit

Here we derive the spectral index analytically for the hilltop inflation limit, $\mu v \gg M_P^2 N_e$. First consider the case where inflation ends at the phase 2-(a) ($c \gg \phi_c^2/(\mu v)$). From Eq. (2·63) and using $|\xi_{\rm end}| \gg |\xi_2'|$, we find

$$\xi(N_{\rm end} - N_e) \simeq -\frac{v^2}{8M_P^2 N_e}, \tag{2·70}$$

and

$$\chi(N_{\rm end} - N_e) \simeq \chi_2 + \ln\left(\frac{\mu v}{4M_P^2 N_e}\right). \tag{2·71}$$

By substituting them into Eqs. (2·5)–(2·9), we obtain

$$\epsilon_\psi(N_e) \simeq 2\epsilon_\phi(N_e) \simeq \frac{\phi_c^2 v^4}{64 M_P^6 N_e^4}. \tag{2·72}$$

This means that both ϕ and ψ significantly contribute to the adiabatic field. Other slow-roll parameters are calculated as

$$\eta_{\phi\phi}(N_e) \simeq \frac{v^2}{8M_P^2 N_e^2}, \tag{2·73}$$

$$\eta_{\phi\psi}(N_e) \simeq \frac{\sqrt{2}}{N_e}, \tag{2·74}$$

$$\eta_{\psi\psi}(N_e) \simeq -\frac{1}{N_e}. \tag{2·75}$$

Therefore, in this limit, the spectral index (2·65) is calculated as

$$n_S \simeq 1 - \frac{4}{N_e}. \tag{2·76}$$

This gives $n_S \simeq 0.92$ for $N_e = 50$ and $n_S \simeq 0.933$ for $N_e = 60$. From this expression it is clear that the spectral index becomes red in this regime. This is seen in Fig. 8.

In the case where the last N_e e-foldings occurs in the phase 2-(b) regime ($\mu v \gg M_P^2 N_e$ and $c \ll \phi_c^2/(\mu v)$), we find

$$\xi(N_{\rm end} - N_e) \simeq -\frac{v^2}{8M_P^2 N_e}, \tag{2·77}$$

and

$$\chi(N_{\rm end} - N_e) \simeq \frac{1}{2} \ln \left(\frac{v^4}{4\psi_0^2 M_P^2 N_e} \right). \tag{2·78}$$

Using them, we obtain the following parameters,

$$\epsilon_\phi \simeq \frac{v^4}{2\phi_c^2 M_P^2 N_e^2}, \quad \epsilon_\psi \simeq 0, \tag{2·79}$$

and

$$\eta_{\phi\phi} \simeq \frac{v^2}{\phi_c^2 N_e}. \tag{2·80}$$

Therefore, the scalar spectral index in this case is given by

$$n_S \simeq 1 + \frac{2v^2}{\phi_c^2 N_e}. \tag{2·81}$$

2.2.2. "Standard" hybrid inflation limit

On the other hand, if $\mu v \ll M_P^2 N_e$, the e-folding number during the waterfall regime is negligibly small and a conventional picture for the hybrid inflation is recovered. In this case, we easily find $\phi(N_e) \simeq \phi_c$ and hence slow-roll parameters are given by

$$\epsilon_\phi(N_e) \simeq \frac{2\phi_c^2 M_P^2}{\mu^4}, \tag{2·82}$$

$$\eta_{\phi\phi}(N_e) \simeq \frac{2M_P^2}{\mu^2}. \tag{2·83}$$

Therefore, the scalar spectral index is given by

$$n_S \simeq 1 + \frac{4M_P^2}{\mu^2} \simeq 1. \tag{2·84}$$

It tends to make the spectral index slightly blue tilted. These features are clearly found in Fig. 8.

2.3. *WMAP normalization and tensor-to-scalar ratio*

So far we have not set the overall inflationary scale, Λ, in Eq. (2·1). It is determined by the condition that the magnitude of the curvature perturbation agrees with the observation. The WMAP normalization reads[6)]

$$\mathcal{P}_\mathcal{R} = \frac{1}{24\pi^2 M_P^4} \frac{V}{\epsilon_\sigma} \simeq 2.4 \times 10^{-9}, \tag{2·85}$$

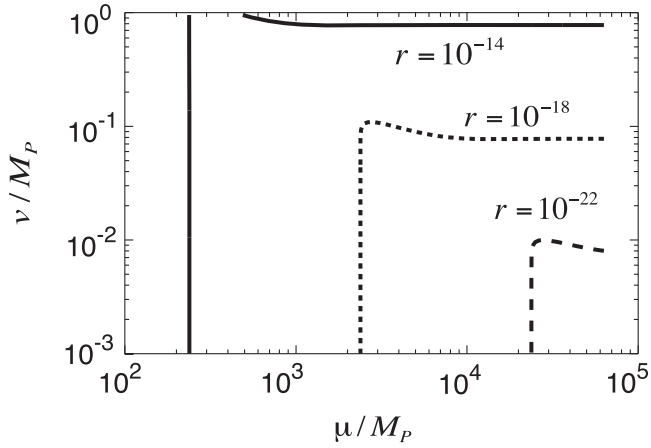

Fig. 9. Contours of the tensor-to-scalar ratio r on (μ, v)-plane. We have taken $\phi_c = 10^{-3} M_P$ and $\psi_0 = 10^{-15} M_P$.

where $\mathcal{P}_\mathcal{R}$ denotes the dimensionless power spectrum of the curvature perturbation at the pivot scale $k = 0.002\ \mathrm{Mpc}^{-1}$. This determines the energy scale of inflation, Λ.

In the hilltop inflation limit, this leads to

$$\Lambda \simeq 2.1 \times 10^{-4} M_P \left(\frac{v}{M_P}\right) \left(\frac{\phi_c}{M_P}\right)^{1/2} \left(\frac{50}{N_e}\right). \tag{2·86}$$

It can also be translated into the tensor-to-scalar ratio, r, defined as the ratio between the power spectrum of the tensor perturbation and $\mathcal{P}_\mathcal{R}$. It is related to the slow-roll parameter as $r = 16\epsilon_\sigma$. Thus we have

$$r \simeq 6.0 \times 10^{-8} \left(\frac{\phi_c}{M_P}\right)^2 \left(\frac{v}{M_P}\right)^4 \left(\frac{50}{N_e}\right)^4. \tag{2·87}$$

In the "standard" hybrid inflation limit, we obtain

$$\Lambda \simeq 3.3 \times 10^{-2} M_P \left(\frac{\phi_c}{M_P}\right)^{1/2} \left(\frac{M_P}{\mu}\right). \tag{2·88}$$

In terms of the tensor-to-scalar ratio r, this gives

$$r \simeq 3.2 \times 10^{-3} \left(\frac{\phi_c}{M_P}\right)^2 \left(\frac{10 M_P}{\mu}\right)^4. \tag{2·89}$$

Contours of r are shown in Fig. 9. Unfortunately, it is so small that future observations will not have a chance to detect it for most of the parameter space.

§3. Conclusions

In this paper, we have reanalyzed the hybrid inflation model, in particular paying attention to the behavior of the waterfall field after the critical point. We have

derived analytic formulae describing the precise motion of both ϕ and ψ fields. In accordance with the result by Clesse,[7] we found that sufficiently long inflation takes place during the waterfall regime for some parameter spaces. Interestingly, in such a case the scalar spectral index tends to be red, as opposed to the well known lore that it becomes blue in the hybrid inflation model, and consistency with current observations becomes better. In this limit, the ψ causes a inflation similar to new inflation. New inflation models often have a problem of initial condition, since initially the inflaton must be placed near the top of the potential. In the present model, it is automatically set around there due to the pre-new inflation dynamics. In this sense, the potential of the hybrid-inflation type (2·1) may be used for the purpose of providing an appropriate initial condition of the new inflation. In this respect, the present model shares a similar property to a model studied e.g. in Ref. 25) in which a period of "pre-inflation" was introduced in order to have an appropriate initial condition for new inflation. What we have shown in this paper is that it is naturally realized in the simple hybrid-type potential (2·1) without introducing any additional field.

If the period of inflation in the waterfall regime is less than 60 e-foldings, it resembles the so-called double inflation, in which some characteristic signatures such as primordial black hole formation and the running of the spectral index are predicted.[26] Although the potential (2·1) can surely cause double inflation, the analysis presented in this paper cannot be applied to such a case and we need careful treatments.[10–15]

Some comments are in order. In general, in the hybrid inflation model topological defects such as domain walls are formed at the waterfall phase transition. In order to avoid the problem of domain walls, we need some additional assumptions. One obvious option is to introduce an additional Z_2-breaking term in the scalar potential, which makes domain walls unstable. Another option is to extend ψ to be a complex scalar and replace ψ in Eq. (2·1) with its absolute value. In this case it is $U(1)$ symmetry that is spontaneously broken after inflation, and correspondingly cosmic strings are formed, which is less harmful than the domain walls. However, in the case where the last 60 e-foldings takes place during the waterfall regime, we do not need such options, since topological defects are inflated away and no such objects exist in the observable region of the Universe. Thus, it has advantages from the viewpoint of not only the spectral index but also the domain wall problem.

Acknowledgements

We would like to thank Fuminobu Takahashi for useful comments on early stage of this project. This work is supported by Grant-in-Aid for Scientific research from the Ministry of Education, Science, Sports, and Culture (MEXT), No. 21111006. K.K. was partly supported by the Center for the Promotion of Integrated Sciences (CPIS) of Sokendai.

Appendix A
— Exact Solution —

A.1. *Phase 0 and Phase 1*

Here we derive analytic solutions for describing both phase 0 and phase 1. In these phases, we have

$$\frac{\sqrt{2}\mu\psi}{\phi_c v} \ll 1, \tag{A·1}$$

but we keep the ψ^2 term in Eq. (2·4). Then the slow-roll equation of motion leads to

$$\frac{d\chi}{d\xi} = \frac{2\mu^2}{v^2}\left(e^{2\xi} - 1 + \frac{\psi_0^2 e^{2\chi}}{v^2}\right). \tag{A·2}$$

Integrating this yields

$$e^{-2\chi} = e^{-2f(\xi)} - \frac{4\psi_0^2\mu^2}{v^4}\int_0^\xi dx e^{-2f(\xi)+2f(x)}, \tag{A·3}$$

under the condition $\chi = 0$ at $\xi = 0$, where

$$f(\xi) = \frac{2\mu^2}{v^2}\int_0^\xi dx(e^{2x} - 1) = \frac{\mu^2}{v^2}(2|\xi| - 1 + e^{-2|\xi|}). \tag{A·4}$$

For $|\xi| \ll v/\mu (\ll 1)$, it is approximated as

$$e^{-2\chi} \simeq 1 + \frac{4\mu^2}{v^2}|\xi|\left(\frac{\psi_0^2}{v^2} - |\xi|\right), \tag{A·5}$$

and for $v/\mu \ll |\xi| \ll 1$, we have

$$e^{-2\chi} \simeq e^{-(2\mu\xi/v)^2} + \frac{\psi_0^2}{2|\xi|v^2}\left(1 - e^{-(2\mu\xi/v)^2}\right). \tag{A·6}$$

It is seen that, starting from $\chi = 0$ and $\xi = 0$, χ decreases first until $|\xi_1| \simeq \psi_0^2/(2v^2)$ if $\psi_0^2 \ll v^3/\mu$, or $|\xi_1| \simeq v/\mu$ if $\psi_0^2 \gg v^3/\mu$, and then increases monotonically. Comparing them with the results of §2.1.1, we find that these solutions smoothly connect our phase 0 and phase 1 solutions. The first term in (A·6) corresponds to the phase 1 solution (2·32). Also notice that the second term in (A·6) comes to dominate during this phase for $\chi_2 < \phi_c^4/(8\mu^2 v^2)$ (phase 1-(b)), and after that the solution coincides with the temporal minimum (2·20). Thus our early claim is confirmed that scalars are trapped at the temporal minimum if $\chi_2 < \phi_c^4/(8\mu^2 v^2)$ by using this exact solution.

A.2. *Phase 2*

Let us seek the solution in the opposite limit,

$$\frac{\sqrt{2}\mu\psi}{\phi_c M} \gg 1, \tag{A·7}$$

without neglecting ψ^2 term in Eq. (2·4). The slow-roll equation of motion leads to

$$\frac{d\chi}{d\xi}e^{2\chi} = \frac{\phi_c^2}{\psi_0^2}\left(e^{2\xi} - 1 + \frac{\psi_0^2 e^{2\chi}}{v^2}\right). \tag{A·8}$$

The solution to this equation is written as

$$e^{2\chi} = \frac{v^2}{\psi_0^2}\frac{1 - e^{2k\xi} - k(1 - e^{2\xi})}{1 - k} + Ce^{2k\xi}, \tag{A·9}$$

where $k \equiv \phi_c^2/v^2$ and C is an arbitrary constant determined from the initial condition. Connecting the phase 1-(a) solution at $\xi_2 = -cv/\mu$, we find the phase 2-(a) solution

$$\begin{aligned} \xi^2 &= \xi_2^2 + \frac{v^2}{4\mu^2}\left(e^{2(\chi-\chi_2)} - 1\right) \quad \text{for} \quad |\xi| \ll \frac{v^2}{\phi_c^2} \ll 1, \\ \xi &= -\frac{\psi_0^2}{2v^2}e^{2\chi} \quad \text{for} \quad \frac{v^2}{\phi_c^2} \ll |\xi| \ll 1 \end{aligned} \tag{A·10}$$

for $\phi_c^4/(\mu^2 v^2) \ll \chi_2 \ll \mu^2 v^2/\phi_c^4$, which coincides with (2·51) and (2·52).

On the other hand, we find a phase 2-(b) solution that connects to phase 1-(b), when $\chi_2 < \phi_c^4/(8\mu^2 v^2)$, as

$$\xi = -\frac{\psi_0^2}{2v^2}e^{2\chi}, \tag{A·11}$$

and hence tracks the temporal minimum, as was already shown in (2·53).

Appendix B
—— *Chaotic Inflation Limit* ——

So far we have focused on the parameter ranges $\phi_c \ll M_P$ and $v \ll M_P$. In the opposite case $\phi_c \gg M_P$ and/or $v \gg M_P$, the scalar potential around the minimum $(\phi, \psi) = (0, v)$ is obviously flat beyond the Planck scale. Thus the final 60 e-folding during the waterfall regime rather looks like chaotic inflation.

We can expand the scalar potential around the minimum by using $\delta\psi \equiv \psi - v$, as

$$V = \frac{1}{2}m_\phi^2\phi^2 + \frac{1}{2}m_\psi^2\delta\psi^2, \tag{B·1}$$

for $|\delta\psi| \ll v$ and $|\phi| \ll \phi_c$, where

$$m_\phi^2 = \frac{2\Lambda^4}{\mu^2} + \frac{4\Lambda^4}{\phi_c^2}, \tag{B·2}$$

$$m_\psi^2 = \frac{8\Lambda^4}{v^2}. \tag{B·3}$$

Therefore, if either $\phi_c \gg M_P$ or $v \gg M_P$ are satisfied, the scalar potential is flat beyond $\phi \sim M_P$ or $|\delta\psi| \sim M_P$, and chaotic inflation along the corresponding direction can take place. In this case, the scalar spectral index and tensor-to-scalar ratio are estimated to be $n_S \sim 0.96$ and $r \sim 0.16$, and the WMAP normalization constrains the mass parameter as $m_\phi(m_\psi) \sim 10^{13}$GeV.

References

1) A. H. Guth, Phys. Rev. D **23** (1981), 347.
K. Sato, Mon. Not. R. Astron. Soc. **195** (1981), 467.
A. A. Starobinsky, Phys. Lett. B **91** (1980), 99.
2) A. Albrecht and P. J. Steinhardt, Phys. Rev. Lett. **48** (1982), 1220.
A. D. Linde, Phys. Lett. B **108** (1982), 389.
3) A. D. Linde, Phys. Lett. B **129** (1983), 177.
4) A. D. Linde, Phys. Lett. B **259** (1991), 38.
5) A. D. Linde, Phys. Rev. D **49** (1994), 748, astro-ph/9307002.
6) E. Komatsu et al., arXiv:1001.4538.
7) S. Clesse, arXiv:1006.4522.
8) K. Kohri, C. M. Lin and D. H. Lyth, J. Cosmol. Astropart. Phys. **12** (2007), 004, arXiv:0707.3826.
9) L. Boubekeur and D. H. Lyth, J. Cosmol. Astropart. Phys. **07** (2005), 010, hep-ph/0502047.
10) D. H. Lyth, arXiv:1005.2461.
11) A. A. Abolhasani and H. Firouzjahi, arXiv:1005.2934.
12) J. Fonseca, M. Sasaki and D. Wands, J. Cosmol. Astropart. Phys. **09** (2010), 012, arXiv:1005.4053.
13) J. O. Gong and M. Sasaki, arXiv:1010.3405.
14) A. A. Abolhasani, H. Firouzjahi and M. H. Namjoo, arXiv:1010.6292.
15) D. H. Lyth, arXiv:1012.4617.
16) E. J. Copeland, A. R. Liddle, D. H. Lyth, E. D. Stewart and D. Wands, Phys. Rev. D **49** (1994), 6410, astro-ph/9401011.
17) G. R. Dvali, Q. Shafi and R. K. Schaefer, Phys. Rev. Lett. **73** (1994), 1886, hep-ph/9406319.
18) A. D. Linde and A. Riotto, Phys. Rev. D **56** (1997), R1841, hep-ph/9703209.
19) V. N. Senoguz and Q. Shafi, Phys. Rev. D **71** (2005), 043514, hep-ph/0412102.
20) M. Bastero-Gil, S. F. King and Q. Shafi, Phys. Lett. B **651** (2007), 345, hep-ph/0604198.
21) K. Nakayama, F. Takahashi and T. T. Yanagida, J. Cosmol. Astropart. Phys. **12** (2010), 010, arXiv:1007.5152.
22) C. Gordon, D. Wands, B. A. Bassett and R. Maartens, Phys. Rev. D **63** (2001), 023506, astro-ph/0009131.
23) D. Wands, N. Bartolo, S. Matarrese and A. Riotto, Phys. Rev. D **66** (2002), 043520, astro-ph/0205253.
24) H. Kodama and T. Hamazaki, Prog. Theor. Phys. **96** (1996), 949, gr-qc/9608022.
25) K. I. Izawa, M. Kawasaki and T. Yanagida, Phys. Lett. B **411** (1997), 249, hep-ph/9707201.
26) M. Kawasaki, N. Sugiyama and T. Yanagida, Phys. Rev. D **57** (1998), 6050, hep-ph/9710259.
T. Kanazawa, M. Kawasaki, N. Sugiyama and T. Yanagida, Phys. Rev. D **61** (2000), 023517, hep-ph/9908350.
M. Yamaguchi, Phys. Rev. D **64** (2001), 063502, hep-ph/0103045; Phys. Rev. D **64** (2001), 063503, hep-ph/0105001.
M. Kawasaki, M. Yamaguchi and J. Yokoyama, Phys. Rev. D **68** (2003), 023508, hep-ph/0304161.